RSC Advances

ROYAL SOCIETY OF CHEMISTRY

www.rsc.org/advances

Cite this: DOI: 10.1039/c0xx00000x

www.rsc.org/xxxxxx

RESEARCH ARTICLE

New insight into rare-earth doped gadolinium molybdate nanophosphor assisted broad spectral converter from UV to NIR for silicon solar cell

Pawan Kumar[a, b] and Bipin Kumar Gupta[a,*]

Received (in xxx) Xth xxxxxxxxx 20xx, Accepted Xth xxxxxxxxx 20xx

DOI: 10.1039/b000000x

We have successfully synthesized rare-earth doped gadolinium molybdate; $Gd_2(MoO_4)_3:Re^{3+}$ (Re^{3+} = Eu^{3+}, Tb^{3+},$Tm^{3+}$and Er^{3+}/Yb^{3+}) nanophosphors for solar cell application as a broad spectral converter from ultraviolet (UV) to near infrared region (NIR) in a single host lattice using facile solid state reaction method. The gross structural analysis, surface morphology and microstructural studies of these nanophosphors have been investigated by x-ray powder diffraction (XRD), scanning electron microscopy (SEM) and transmission/high-resolution transmission electron microscopy techniques (TEM/HRTEM), respectively. The photoluminescence (PL) and time-resolved spectroscopic (TRPL) methods have been used to explore the striking luminescence properties of synthesized nanophosphors. The $Gd_2(MoO_4)_3:Eu^{3+}$ nanophosphor exhibits hypersensitive red emission (616 nm) at excitation wavelength in range of 250-475 nm corresponding to $^5D_0$-$^7F_2$ transition. The $Gd_2(MoO_4)_3:Tb^{3+}$ and $Gd_2(MoO_4)_3:Tm^{3+}$nanophosphors demonstrate strong green emission at 541 nm and deep blue emission at 453 nm upon excitation wavelength of 378 nm and 266 nm, respectively. Moreover, upconversion characteristic of $Gd_2(MoO_4)_3:Er^{3+}/Yb^{3+}$ nanophosphor exhibits the strong green emission at 545 nm and red emission at 657 nm corresponding to $^4S_{3/2}$-$^4I_{15/2}$ and $^4F_{9/2}$-$^4I_{15/2}$ transitions respectively. Furthermore, $Gd_2(MoO_4)_3:Er^{3+}/Yb^{3+}$upconversionnanophosphor emits in NIR spectrum region at 994 nm upon 980 nm excitation wavelength. Hence, the obtained PL emission results with lifetime in millisecond reveal that these nanophosphors could be futuristic promising broad spectral converter phosphor which may possibly integrate with the next-generation Si-solar cell to enhance the efficiency of the cell.

1. Introduction

Energy is directly related to the currency of any country. No, doubt, it is always in huge demand, but unluckily, always in short supply and insufficient to match the unparalleled population explosion and our changing comfort lifestyle. Undeniably, we are facing an energy crises and it has become the most important commodity. The energy consumption will be almost doubled in 2050 as compare to the energy consumption in 2001.[1-2]Consequently, the renewable energy sources which can provoke the sufficient energy to meet worldwide energy demand have attained huge attention.[1-5]The sunlight is most important out of all renewable source of energy which can directly convert into heat and electricity. Moreover, sunlight is plentiful source of energy; available almost everywhere in word without any cost.[5]The photovoltaic cell which converts sunlight directly into electricity is a most prominent renewal source of energy. But, the photovoltaic cell is contributing limited portion of energy demand. Therefore, over past decades, the significant efforts have been done to development of efficient photovoltaic cell. Still, the efficient and economic cost conversion of sunlight into electricity remains a challenging task.[6-8]Therefore, the photovoltaic cell is contributing limited portion of energy demand. Commercial availability and economic approach of crystalline and polycrystalline solar cell are dominating photovoltaic market till date.[9-10] Therefore, the immense research has been devoted to developed efficient and low cost crystalline and polycrystalline solar cell in past few decades.

A major drawback of Si-solar cell exists that it doesn't utilize full solar spectrum during falling the sunlight on the surface Si-solar cell which limits its energy conversion efficiency. It is well established that the solar spectrum has photons ranging for 250-2500 nm (ultra violet to infrared) at air mass 1.5 global (AM 1.5G). But, photovoltaic cell only utilized a small portion of solar spectrum which is attributed only photons that match to the band gap of material.[11]In general; there are two kind of loss in solar cell that limits its efficiency. One is the photons having energy higher than band gap (UV radiations) are not efficiently used; the excess energy of photons is dissipated in form of heat. Secondly, the photons with low energy (IR radiation) are not absorbed by solar cell and these are transmitted. It is observed that the 70%

losses in solar cell are related to these losses known as spectral mismatch. One of the promising way to address this issue by using the downshift (DS) or upconversion(UC) materials as a spectral converter to minimise these losses (thermalisation and non-absorbed losses). The downshift material can absorbed the photons having high energy and emits photons having lower energy in visible which are subsequently absorbed by solar cell without any heat dissipation. Upconversion materials absorbed two photons having energy less than band gap of solar cell and converted into a utilized photon (having energy in visible spectrum region) which is absorbed by solar cell. This approach to minimise the thermalisation and non-absorbed losses by applying luminescent layer on solar cell is termed as third generation solar conversion.[5]Although, there are many materials have been proposed as luminescent concentrator for the enhancement of solar cell efficiency. The lanthanides doped materials are most suitable materials for solar spectral converter due to their electron rich energy level structure which offer a superficial photon management. Therefore, significant effort have been dedicate for enhanced the efficiency of solar cell via modification of solar spectrum using trivalent lanthanide doped materials.[12-23]

Among various trivalent lanthanides ions (Ln^{3+}), the materials doped with Eu^{3+}/Er^{3+} ions (downshift/upconversion phosphors) have gained more inquisitiveness as a spectral converter. These materials can emit photons in visible spectrum which are useful in solar cell application to create electron-hole pair. Moreover, the host lattice containing d-block transition element (like tungstate and molybdate) have advantage over other host lattice that the excitation band is broad due the charge transfer (CT) in O-Mo or O-W bond in UV region, which is sufficiently transferred to trivalent lanthanide ion.[24]Further, the $Gd_2(MoO_4)_3$ host matrix possess beneficial properties such as high refractive index, high thermal stability, low toxicity and high photochemical stability.

In present investigation, we have synthesized $Gd_2(MoO_4)_3:Re^{3+}$ (Re^{3+} =Eu^{3+}, Tb^{3+},Tm^{3+},Er^{3+}/Yb^{3+}) nanophosphors for proposed solar cell application where these nanophosphors act as a spectral converter nanophosphor. These nanophosphors have capability to absorb light in broad range from UV to IR and can be emit red, green and blue emission in visible and NIR regions. The $Gd_2(MoO_4)_3:Eu^{3+}$ downshift nanophosphor demonstrates that the photoluminescence emission peak at 616 nm (hypersensitive red emission) upon broad excitation ranging from 250-475 nm. Moreover, other two downshift nanophosphors $Gd_2(MoO_4)_3:Tb^{3+}$ and $Gd_2(MoO_4)_3:Tm^{3+}$ exhibit the emission peaks at 541 nm and 453 nm which represent strong green and deep blue emission, respectively. Furthermore, the upconversion $Gd_2(MoO_4)_3:Er^{3+}/Yb^{3+}$ nanophosphor shows strong green emission at 545nm and red emission at 657 nm, respectively.

Additionally, the $Gd_2(MoO_4)_3:Er^{3+}/Yb^{3+}$ upconversion nanophosphor exhibits emission at 994 nm (NIR region) upon 980 nm excitation wavelength, which is merely reported in literature. Thus, $Gd_2(MoO_4)_3:Re^{3+}$ (Eu^{3+}, Tb^{3+},Tm^{3+},Er^{3+}/Yb^{3+}) nanophosphors could be efficiently used as a spectral converter, which can absorbed light in 250-475 nm/NIR spectrum region and could emit in visible and NIR region which is highly desired for the modification of Si-solar cell spectrum. Hence, the obtained result provides a new podium of $Gd_2(MoO_4)_3:Re^{3+}$ (Re^{3+}= Eu^{3+}, Tb^{3+},Tm^{3+}, Er^{3+}/Yb^{3+}) nanophosphors to examine in details about its interesting photoluminescence properties for proposed Si-solar cell applications .

2. Experimental

2.1 Materials

The precursores; Y_2O_3 (99.99%), Eu_2O_3 (99.99%), Tm_2O_3(99.99%), $Tb_{24}O_7$ (99.99%), $Er(NO_3)_3{:}5H_2O$ (99.99%), Yb_2O_3(99.99%) and $(NH_4)_6Mo_7O_{24}{:}4H_2O$ (AR grade, 99%) were purchased from Sigma-Aldrich. All reagents were of analytical (AR) grade and used as received without further purification.

2.2 Synthesis of $Gd_2(MoO_4)_3:Re^{3+}$(Re^{3+}=Eu^{3+}, Tb^{3+}, Tm^{3+}, Er^{3+}/Yb^{3+}) Nanophosphor:

A facile solid state reaction was used for the synthesis of $Gd_2(MoO_4)_3:Re^{3+}$(Re^{3+} = Eu^{3+}, Tb^{3+}, Tm^{3+}, Er^{3+}/Yb^{3+}) which can be easily scaled-up in large quantities. In order to optimized the concentration and temperature, first we have synthesized the red emitting $Gd_{2-x}(MoO_4)_3:Eu_x^{3+}$ (x = 0.1 to 0.5) nanophosphor using solid state reaction method. According to stoichiometric ratio, the starting materials: Gd_2O_3, Eu_2O_3, and $(NH_4)_6Mo_7O_{24}{:}4H_2O$ were taken. After precise weighting of these materials, the materials were properly crushed in an agate mortar for homogeneous mixing. Further, the homogeneous mixture was kept into an alumina crucible and heated in a box furnace at the temperature of 1000^{o}C for 3hrs. The doping concentration of Eu^{3+}(x=0.1 to 0.5) was varied in order to attain the optimum dopant concentration for strongest red emission and it is observed that the x= 0.2 is the optimum concentration. Furthermore, in order to compare the luminescence intensity with sintering temperature, $Gd_{1.8}(MoO_4)_3:Eu^{3+}$phosphor was heated at 800^{o}C, 900^{o}C, 1000^{o}C and 1100^{o}C, respectively. The green and blue nanophosphors were also synthesized by doping different rare-earth ions (Tb^{3+} and Tm^{3+}). The Tb^{3+} was doped to achieve the green emission and Tm^{3+} for blue emission. Similarly, the upconversion nanophosphor $Gd_2(MoO_4)_3:Er^{3+}/Yb^{3+}$($Er^{3+}$=5 mol% and Yb^{3+}= 10 mol%) have also been synthesized by solid state reaction method keeping same ambient as for downshift nanophosphor. In this method, the yield of material is more than 90% in all cases (downshift and upconversion nanophosphors) with a high degree of homogeneity throughout the mass. The versatility of this method is such that one could easily synthesized large quantities of homogeneous rare earth doped nanophosphor with a narrow size distribution.

2.3 Characterization

The crystal structure analysis was investigated by using x-ray powder diffraction (XRD) with Bruker AXS D8 Advance x-ray diffractometer, using Cu $K\alpha_1$ radiation (λ = 1.5406 Å). The surface morphology was studied by using Carl ZEISS EVOR-18 equipment at 10 kV operating voltage. Transmission electron microscopy (TEM) and high-resolution transmission microscopy micrographs (HRTEM) were recorded by using Tecnai G2 S-Twin transmission electron microscope with a field emission gun operating at 300 kV. The Edinburgh spectrometer was used for photoluminescence (PL) and time-resolved photoluminescence (TRPL) spectroscopy, where xenon lamp acts as source of excitation. To estimate the absolute luminescence quantum efficiency of the QC phosphors, an integrating sphere equipped with an Edinburgh spectrometer (model F900) instrument has been used, and then by measuring the integrated fraction of luminous flux and radiant flux with the standard method, quantum efficiency has been evaluated. The NIR PL emission and PL mapping of nanophosphor was performed using a WITech alpha 300R+ confocal PL microscope system, where 375 and 980 nm diode laser act as source of excitations.

3. Results and discussion

A facile solid state reaction method has been used to the synthesis of $Gd_2(MoO_4)_3:Re^{3+}$ (Re^{3+}=Eu^{3+}, Tb^{3+}, Tm^{3+}, Er^{3+}/Yb^{3+}).The x-ray diffraction (XRD) technique has been carried out for the gross structural investigation and phase purity of nanophosphor. The XRD pattern of $Gd_{1.8}(MoO_4)_3:Eu_{0.2}^{3+}$downshift nanophosphor is illustrated in Fig. 1(a). The XRD result reveals that the nanophosphor has orthorhombic crystalline structure with space group Pba2. The estimated lattice parameters for the $Gd_{1.8}(MoO_4)_3:Eu_{0.2}^{3+}$ nanophosphor are a = (10.1631±0.0023)Å, b= (10.1132±0.0021)Å and c= (10.74±0.0027)Å, which is comparable with the existing $Gd_2(MoO_4)_3$host (JCPDS card no.20-0408). The estimated crystallite size of $Gd_{1.8}(MoO_4)_3:Eu_{0.2}^{3+}$ nanophosphor is ~28 nm using standard Scherrer formula. The XRD patterns of $Gd_{2-x}(MoO_4)_3:Eu_x^{3+}$downshift nanophosphor for different concentrations (x=0.1 to 0.5) are demonstrated in Fig. S1 (see supporting information).The lattice parameters for all the variants of $Gd_{2-x}(MoO_4)_3:Eu_x^{3+}$ nanophosphors, (x = 0.1 to 0.5) were calculated from the observed d-values through a least square fitting method using computer program based unit cell refinement software.[25] The unit cell volume is estimated from these parameters and exhibited in Table S1. It is observed that the unit cell volume increases for the Eu^{3+}-doping concentration up to a value of 0.2 and then after this it started to decrease. The decrease in unit cell volume decreases the inter-ionic distance between the Eu^{3+} ions which leads to increase in non-radiative emission which decreases luminescence intensity. Furthermore, the obtained results of different concentrations (x=0.1 to 0.5) of $Gd_{2-x}(MoO_4)_3:Eu_x^{3+}$ nanophosphors with their unit cells parameters are in consistent with obtained PL emission results. Therefore, the emission intensity is maximum for doping concentration x= 0.2. The Fig. S2 exhibit the XRD patterns of $Gd_{1.8}(MoO_4)_3:Eu_{0.2}^{3+}$downshift nanophosphor at different sintering temperature (800°C, 900°C, 1000°C and 1100°C)[26]. The obtain XRD patterns of $Gd_{1.8}(MoO_4)_3:Eu_{0.2}^{3+}$ nanophosphor at different sintering temperature reveals that the relative peak intensity of $Gd_{1.8}(MoO_4)_3:Eu_{0.2}^{3+}$ increases when the sintering temperature increases from 800 to 1000 °C and above 1000 °C , the secondary phases start to appear as result it affects the PL intensity of $Gd_{1.8}(MoO_4)_3:Eu_{0.2}^{3+}$nanophosphor, which is further discussed in details in PL section. The Fig. 1(b) demonstrates the XRD pattern of $Gd_2(MoO_4)_3:Er^{3+}/Yb^{3+}$ upconversion nanophosphor. The XRD patterns of $Gd_{1.8}(MoO_4)_3:Tb_{0.2}^{3+}$ and $Gd_{1.8}(MoO_4)_3:Tm_{0.2}^{3+}$ downshift nanophosphors is also illustrated in Fig. S3 (see supporting information).

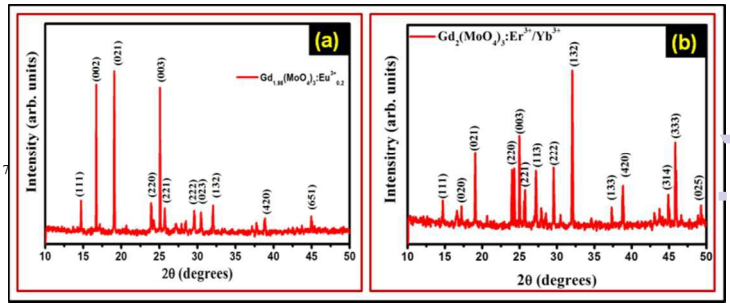

Fig. 1: The XRD pattern of (a) $Gd_{1.8}(MoO_4)_3:Eu_{0.2}^{3+}$ downshift nanophosphor and (b)$Gd_2(MoO_4)_3:Er^{3+}/Yb^{3+}$ upconversion nanophosphor.

The scanning electron microscopy (SEM) has been used to explore the investigations on the surface morphology of synthesized nanophosphors. Fig. 2(a) exhibits the SEM image of $Gd_{1.8}$ $(MoO_4)_3:Eu_{0.2}^{3+}$downshift nanophosphor. For the more details about the microstructure analysis of $Gd_{1.8}(MoO_4)_3:Eu_{0.2}^{3+}$nanophosphor, transmission electron microscopy (TEM) and the high-resolution transmission electron microscopy (HRTEM) has been performed. The TEM of $Gd_{1.8}(MoO_4)_3:Eu_{0.2}^{3+}$downshift nanophosphor is demonstrated in Fig. 2(b). The TEM image shows that the average particle size of nanophosphor is ~24 nm. The size distribution histogram of $Gd_{1.8}(MoO_4)_3:Eu_{0.2}^{3+}$ downshift nanophosphor is shown in Fig. S4 (see supporting information).The HRTEM image of selected individual nanoparticle (marked in Fig. 2(b)) has also been shown in Fig. 2 (c). The Fig. 2(d) represents that the HRTEM image of nanophosphor which exhibits the clear lattice fringes without any distortion, which confirms that the nanophosphor has good crystal quality. The estimated d-spacing is precisely measured ~ 0.46 nm from Fig. 2 (d), which is analogous to the d-spacing corresponding (021) plane (JCPDS card no. 20-0408). Moreover, the selected area electron diffraction (SAED) pattern of $Gd_{1.8}(MoO_4)_3:Eu_{0.2}^{3+}$nanophosphor is also performed. The Fig. S5 (see supporting information) demonstrates the SAED pattern of $Gd_{1.8}(MoO_4)_3:Eu_{0.2}^{3+}$ which clearly exhibits that nanophosphor is highly crystalline. Further, the energy dispersive x-ray analysis (EDAX) analysis was performed for the element detection. The Fig. S6 (see supporting information) EDAX spectrum of $Gd_2(MoO_4)_3:Eu^{3+}$ nanophosphor which conform the presence of Gd, Mo, O and Eu elements. Moreover, the element analysis for the upconversion nanophosphor is also performed. The EDAX spectrum of $Gd_2(MoO_4)_3:Er^{3+}/Yb^{3+}$ upconversion nanophosphor is shown in Fig. S7(see supporting information) which conform the presence of Gd, Mo, O, Er and Yb elements.

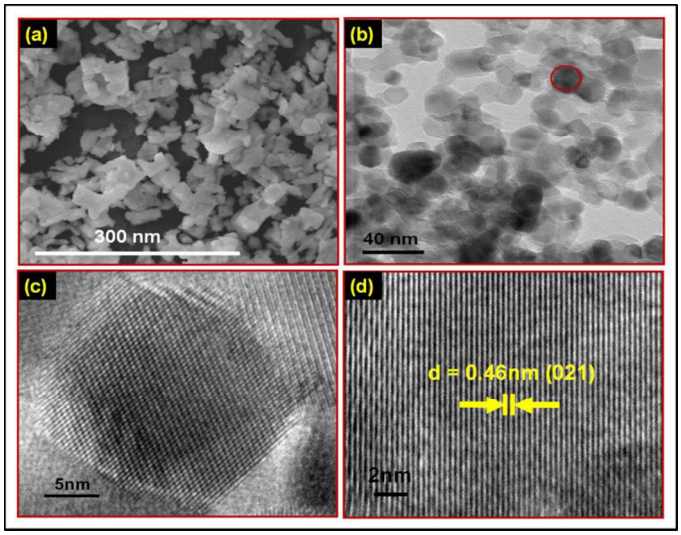

Fig. 2: (a) The SEM image of $Gd_{1.8}(MoO_4)_3:Eu_{0.2}^{3+}$ downshift nanophosphor, (b) TEM image of $Gd_{1.8}(MoO_4)_3:Eu_{0.2}^{3+}$ downshift nanophosphor, (c) the typical HRTEM image of selected individual particle which is marked by red circle in (b), and (d) the HRTEM image of $Gd_{1.8}(MoO_4)_3:Eu_{0.2}^{3+}$ downshift nanophosphor which exhibits the clear lattice fringes without any distortion.

Further, the PL and TRPL have been carried out to explore the spectroscopic characteristic of synthesized nanophosphor to examine the feasibility of this nanophosphor for proposed spectral converter application. The photoluminescence excitation (PLE) spectrum of $Gd_{1.8}(MoO_4)_3:Eu_{0.2}^{3+}$downshift nanophosphor is illustrated in Fig. 3(a). The excitation spectrum has a broad band around 290 nm and sharp peaks in range of 350-475 nm. The broad band ~290 nm is due to the energy charge transfer between Mo-O. It is well known that the transition metal containing host matrix(like VO_4^{3-}, NbO_4^{3-} ,WO_4^{2-}- and MoO_4^{2-} group containing host matrix) have additional advantage over the other host matrix that the scan absorb broad range in UV spectrum region due to the charge transfer between the electron deficient transition metal ion and electron rich oxygen ion.[24,27] Therefore, the energy transfer between the transition metal atom and oxygen is very important factor to enhance the luminescent properties of inorganic phosphor. The sharp peaks are characteristics of the f-f transition within $4f^6$ electron shell of Eu^{3+} ion in the host lattices. The two strong excitation peaks at 395 nm and 465 nm is attributed to the $^7F_0$-$^5L_6$ and $^7F_0$-$^5D_2$ transitions of Eu^{3+} ion, respectively.[28] The Fig. 3(b) depicts the emission spectrum of $Gd_{1.8}(MoO_4)_3:Eu_{0.2}^{3+}$downshift nanophosphor at excitation wavelength 395 nm. The emission spectrum shows hyperfine red emission at 616 nm with quantum efficiency ~84%. The emission peaks at 589 nm, 596 nm, 616 nm, 623 nm and 701nm are attributed to$^5D_0$-$^7F_1$, $^5D_0$-$^7F_1$, $^5D_0$-$^7F_2$, $^5D_0$-$^7F_2$ and$^5D_0$-$^7F_4$ transition, respectively. The strong red emission of nanophosphor has been obtained by optimising the doping concentration of Eu^{3+} ion. Fig. 3 (c) reveals the variation in luminescence intensity with doping concentration of Eu^{3+} ion. It has been observed that the luminescence intensity increases with increase in doping concentration of Eu^{3+}up to 10 mol%. However, with furthermore increase the Eu^{3+}concentration, the luminescence intensity start decreases and it decrease rapidly after 20 mol% concentration. The decrease in luminescence intensity with increase in Eu^{3+}concentration is due to the decrease in distance between two Eu^{3+} ions in host matrix. This decreases in distance between the Eu^{3+} ions reduces the probabilities of the radiative transitions of Eu^{3+} ions due to the mutually interaction the shortened distances between two Eu^{3+} ions at high doping concentration and its leads to non-radiative emission which decreases luminescence intensity. Therefore, obtain result suggests that the 10 mol% concentration is optimised doping concentration. Besides, the $Gd_{1.8}(MoO_4)_3:Eu_{0.2}^{3+}$nanophosphor has been sintered at different temperature (800 to 1100°C) for optimization the sintering temperature for luminescent intensity. The variation in luminescence intensity with sintering temperature has been shown in Fig. S8 (see supporting information). It has been observed that 1000°C is optimum temperature having highest luminescent intensity. Further, the PL emission intensity of $Gd_{1.8}(MoO_4)_3:Eu_{0.2}^{3+}$ downshift nanophosphor is decreases at 1100°C and above. The decrease in PL emission intensity at 1100°C is due the formation of secondary phases at high temperature which was earlier observed in XRD pattern of $Gd_{1.8}(MoO_4)_3:Eu_{0.2}^{3+}$ downshift nanophosphor at 1100°C. The Fig. 3 (d) exhibits the emission spectra of $Gd_{1.8}(MoO_4)_3:Eu_{0.2}^{3+}$downshift nanophosphor at different excitation wavelength. It exhibits that 395 nm excitation wavelength has maximum emission intensity which signify that 395 nm is prominent excitation wavelength for maximum emission intensity. The purposed energy level diagram for $Gd_{1.8}(MoO_4)_3:Eu_{0.2}^{3+}$ downshift nanophosphor have been illustrated in Fig. S9 (see supporting information) which explicated the downshift mechanism for luminescence process in $Gd_{1.8}(MoO_4)_3:Eu_{0.2}^{3+}$nanophosphor.

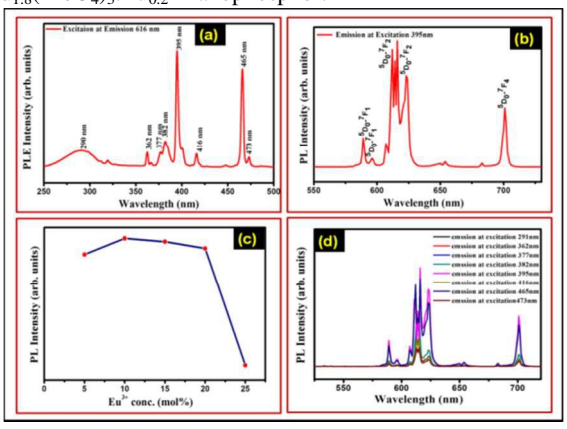

Fig. 3:(a) the excitation spectrum of $Gd_{1.8}(MoO_4)_3:Eu_{0.2}^{3+}$ downshift nanophosphor at emission 616 nm, (b) the PL emission spectrum with quantum efficiency ~84% of $Gd_{1.8}(MoO_4)_3:Eu_{0.2}^{3+}$ downshift nanophosphor at excitation 395 nm wavelength, (c) PL intensity variation with doping concentration of Eu^{3+}in $Gd_{2-x}(MoO_4)_3:Eu_x^{3+}$downshift nanophosphor and (d) PL emission spectra of $Gd_{1.8}(MoO_4)_3:Eu_{0.2}^{3+}$ downshift nanophosphor at different excitation wavelength.

Moreover, the photoluminescence properties of $Gd_{1.8}(MoO_4)_3:Tb_{0.2}^{3+}$ and $Gd_{1.8}(MoO_4)_3:Tm_{0.2}^{3+}$ downshift nanophosphors have been also carried out to explore the spectroscopic characteristic of synthesized nanophosphor to examine the feasibility of this nanophosphor with different dopant for proposed spectral converter application. The Fig. S10 (see supporting information) exhibits the photoluminescence properties of $Gd_{1.8}(MoO_4)_3:Tb_{0.2}^{3+}$ and $Gd_{1.8}(MoO_4)_3:Tm_{0.2}^{3+}$ downshift nanophosphors. The Fig. S10(a) demonstrates the emission spectrum of $Gd_{1.8}(MoO_4)_3:Tb_{0.2}^{3+}$ downshift nanophosphor having strong green emission at 541nm upon 378 nm excitation wavelength. Fig. S10(b) demonstrate the excitation spectrum of $Gd_{1.8}(MoO_4)_3:Tb_{0.2}^{3+}$ downshift nanophosphors at emission 541nm. The emission spectrum of $Gd_{1.8}(MoO_4)_3:Tm_{0.2}^{3+}$ downshift nanophosphor is illustrated in Fig. S11(c). The emission spectrum of $Gd_{1.8}(MoO_4)_3:Tm_{0.2}^{3+}$ downshift nanophosphor shows hypersensitive blue emission at 453 nm upon 266 nm excitation wavelength. Fig. S10 (d) reveals the excitation spectrum of $Gd_{1.8}(MoO_4)_3:Tm_{0.2}^{3+}$ downshift nanophosphors at emission 453 nm,. The TRPL technique is an imperative and non-destructive tool which has been used to determine the decay lifetime of nanophosphor. The lifetime data of nanophosphor is very important and it help to decide the suitable application of nanophosphor applications. The Fig.S11(a) (see supporting information) demonstrates the decay profile of $Gd_{1.8}(MoO_4)_3:Eu_{0.2}^{3+}$ downshift nanophosphor at emission 616 nm upon 395 nm excitation wavelength for $^7F_0$-$^5D_2$ transitions of Eu^{3+} ion. The inset in Fig. S11(a) exhibits the exponential fitting parameters of decay profile of $Gd_{1.8}(MoO_4)_3:Eu_{0.2}^{3+}$ downshift nanophosphor. The decay profile has been best fitted to the double exponential function as described in equation (1). [29]

$$I(t)=A_1\exp(-t/\tau_1)+A_2\exp(-t/\tau_2) \quad (1)$$

Where τ_1 , τ_2, A_1 and A_2 are the decay lifetimes of the luminescence and weighting parameters, respectively.

The obtained parameters after double exponential fitting are listed in inset of Fig. S11 (a). The decay lifetimes of $Gd_{1.8}(MoO_4)_3:Eu_{0.2}^{3+}$ downshift nanophosphor are τ_1 ~ 0.56 ms and τ_2 ~ 0.81ms. The average decay lifetime of $Gd_{1.8}(MoO_4)_3:Eu_{0.2}^{3+}$ nanophosphor is τ_{av}~0.64 ms which is measured using equation (2) as described below.

$$\tau_{av} = (A_1\tau_1^2 + A_2\tau_2^2)/(A_1\tau_1 + A_2\tau_2) \quad (2)$$

Therefore, the achieved PL and TRPL results suggest that $Gd_{1.8}(MoO_4)_3:Re_{0.2}^{3+}$($Re^{3+}$ = Eu^{3+}, Tb^{3+} and Tm^{3+}) downshift nanophosphor is meet the stringent criteria of Si-solar cell and it is highly suitable for Si-solar cell as well as other display and biological applications. The CIE colour co-ordinates of $Gd_{1.8}(MoO_4)_3:Re_{0.2}^{3+}$($Re^{3+}$ = Eu^{3+}, Tb^{3+} and Tm^{3+}) are exhibited in Fig. S11 (b) (see supporting information). The symbolic marks A (x=0.66, y=0.33), B (x=0.34, y=0.60) and C (x=0.14, y=0.11) demonstrate the CIE colour co-ordinates for $Gd_{1.8}(MoO_4)_3:Eu_{0.2}^{3+}$, $Gd_{1.8}(MoO_4)_3:Tb_{0.2}^{3+}$ and $Gd_{1.8}(MoO_4)_3:Tm_{0.2}^{3+}$ emission, respectively.

In order to explore the upconversion nature of $Gd_2(MoO_4)_3:Er^{3+}/Yb^{3+}$ nanophosphor, we have also performed the PL spectroscopy of synthesized upconversion nanophosphor. Conceptually, the upconversion is a process in which the consecutive absorption of two photons of lower energy (IR spectrum region) and emission of a higher energy photon (visible spectrum region).[30]The upconversion materials are particular in interest for solar cell application because these materials are utilized of IR spectrum region of the solar spectrum which is transmitted by solar cell.[15,31-36]The emission spectrum $Gd_2(MoO_4)_3:Er^{3+}/Yb^{3+}$upconversion nanophosphor upon excitation wavelength 980 nm have been demonstrated in Figs. 4 (a &b).Fig.4 (a) exhibits the strong green emission at 545 nm and red emission at 657 nm, which are attributed to $^4S_{3/2}$-$^4I_{15/2}$ and $^4F_{9/2}$-$^4I_{15/2}$ transitions, respectively. Additionally, the emission spectrum also demonstrates a weak emission centred at wavelength 525 nm attributed to $^2H_{11/2}$-$^4I_{15/2}$transition. Moreover, $Gd_2(MoO_4)_3:Er^{3+}/Yb^{3+}$upconversion nanophosphor has strong emission at 994 nm, as shown in Fig. 4(b), which is merely reported in literature so far as per best of our knowledge. This emission is also efficiently contributing to enhance the solar cell efficiency because of the fact that the energy of these photons are very near to the band gap of solar cell. The CIE colour co-ordinates of $Gd_2(MoO_4)_3:Er^{3+}/Yb^{3+}$ nanophosphor corresponding to upconversion emission at 980 nm excitation wavelength is exhibited in Fig. 4(c) with values x=0.29 and y= 0.68.

The Fig. 4(d) represents the schematic diagram for upconversion process in $Gd_2(MoO_4)_3:Er^{3+}/Yb^{3+}$ nanophosphor. In $Gd_2(MoO_4)_3:Er^{3+}/Yb^{3+}$upconversion nanophosphor, Yb^{3+} ion act as sensitizer and Er^{3+} used as dopant, which provide the emission. The Yb^{3+} is used for sensitizer because it can absorb broad NIR region as compared to the Er^{3+} ion. In case of upconversion, both Yb^{3+} and Er^{3+} ions absorbed incident photons of 980 nm wavelength.

However, absorption across the $^2F_{7/2}$-$^2F_{5/2}$ transition in Yb^{3+} ion has more photons compare to absorption across the $^4I_{15/2}$-$^4I_{11/2}$ transition in case of Er^{3+} ion. Therefore, Yb^{3+} ion absorbed most off the incident photons. Furthermore, Yb^{3+} ion also can sufficiently transfer energy to Er^{3+} because energy of $^2F_{5/2}$ level in Yb^{3+} ion is similar to energy of $^4I_{11/2}$ level of Er^{3+} ion.[28] The excited Yb^{3+} ion relax to ground state and transfer energy to neighbour Er^{3+} ion. Therefore, the excited Er^{3+} ion absorb energy for Yb^{3+} ion and promoted to higher excitation state which increase the population in higher energy state. Otherwise, Er^{3+} ion can absorbed simultaneously two low energy photons and which drives Er^{3+} to higher energy state. The excited Er^{3+} ion relax to ground state produces upconversion and emits strong green colour emission corresponding to $^4S_{3/2}$-$^4I_{15/2}$ transition whereas red emission in case of $^4F_{9/2}$-$^4I_{15/2}$ transition.

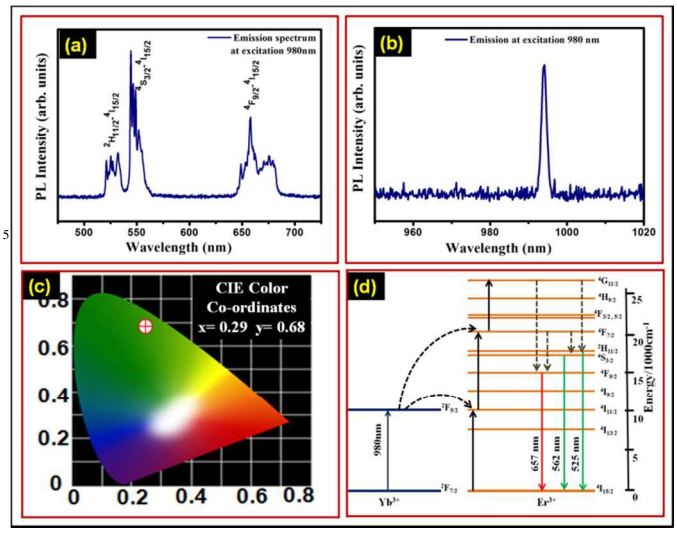

Fig.4: (a) and (b) the emission spectra (range 450-750 and 900-1020)of $Gd_2(MoO_4)_3:Er^{3+}/Yb^{3+}$upconversion nanophosphor at excitation wavelength 980 nm, (c) the CIE colour co-ordinates of $Gd_2(MoO_4)_3:Er^{+}/Yb^{3+}$upconversion nanophosphor which exhibits a green emission and (d) the schematic for proposed upconversion process in $Gd_2(MoO_4)_3:Er^{3+}/Yb^{3+}$ nanophosphor.

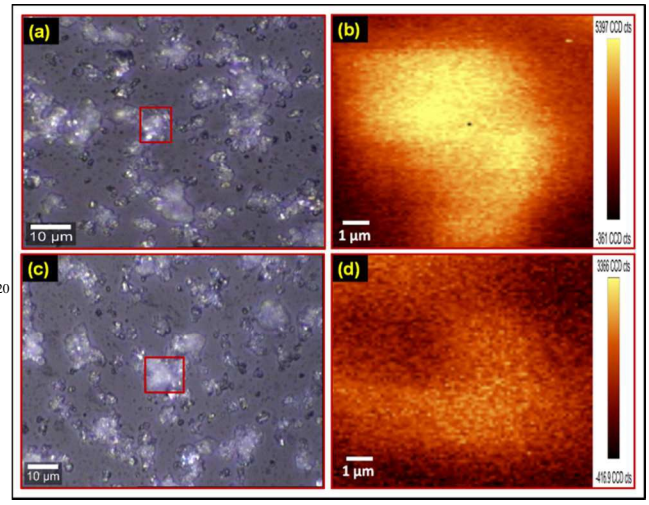

Fig. 5: (a) optical image of $Gd_{1.8}(MoO_4)_3:Eu_{0.2}^{3+}$ downshift nanophosphor on glass slide, (b) the PL mapping image of the selected region (marked by red square in Fig (a)) $Gd_{1.8}(MoO_4)_3:Eu_{0.2}^{3+}$ downshift nanophosphor excited at excitation wavelengths of 375 nm. (c) optical image of $Gd_2(MoO_4)_3:Er^{3+}/Yb^{3+}$ upconversion nanophosphor on glass slide, (d) the PL mapping image of the selected region (marked by red square in Fig (c)) $Gd_2(MoO_4)_3:Er^{3+}/Yb^{3+}$ upconversion nanophosphor excited at excitation wavelengths of 980 nm.

Furthermore, the PL emissions of $Gd_2(MO_4)_3:Eu^{3+}$and $Gd_2(MoO_4)_3:Er^{3+}/Yb^{3+}$ nanophosphor are also compare with other similar host systems with same dopants ($GdPO_4$: Eu^{3+} , $GdBO_3$: Eu^{3+}, $GdPO_4$: Er^{3+}/Yb^{3+} and $GdBO_3$: Er^{3+}/Yb^{3+}). The Fig. S12 (a) (see supporting information) demonstration the emission spectra of $Gd_2(MO_4)_3:Eu^{3+}$, $GdPO_4$: Eu^{3+} and $GdBO_3$: Eu^{3+}downshift nanophosphor under the excitation wavelength 395 nm. The Fig. S12 (b) (see supporting information) exhibits the emission spectra of $Gd_2(MoO_4)_3:Er^{3+}/Yb^{3+}GdPO_4$: Er^{3+}/Yb^{3+} and $GdBO_3$: Er^{3+}/Yb^{3+}upconversion nanophosphor at excitation wavelength 980 nm. The obtain result are shown in Fig. S12 reveals that $Gd_2(MO_4)_3$host lattice based nanophosphor have high emission in both downshift as well as upconversion which is may be due to efficient energy transfer from host lattice to activator as compared to other similar host lattice systems.

Moreover, the PL mapping of downshift as well as upconversion nanophosphors are performed for the conformation of uniform emission from nanophosphor. Fig. 5 (a) exhibits the optical image of $Gd_{1.8}(MoO_4)_3:Eu_{0.2}^{3+}$ downshift nanophosphor on glass slide. The PL mapping of red mark area in optical image Fig. 5 (a) under exciation wavelength 375 nm is demonstrates in Fig. 5(b). The Fig. 5 (b) clearly shows that the nanophosphor have uniform PL emission from nanophosphor. The optical image of $Gd_2(MoO_4)_3:Er^{3+}/Yb^{3+}$ upconversion nanophosphor is illustrated in Fig. 5 (c). The Fig. 5(d) reveals the PL mapping image of $Gd_2(MoO_4)_3:Er^{3+}/Yb^{3+}$ upconversion nanophosphor of marked region in Fig. 5 (c) under excitation wavelength 980 nm. The obtained result reveals the uniform distribution of photoluminescence emission intensity in $Gd_{1.8}(MoO_4)_3:Eu_{0.2}^{3+}$ downshift as well as $Gd_2(MoO_4)_3:Er^{3+}/Yb^{3+}$ upconversion nanophosphors.

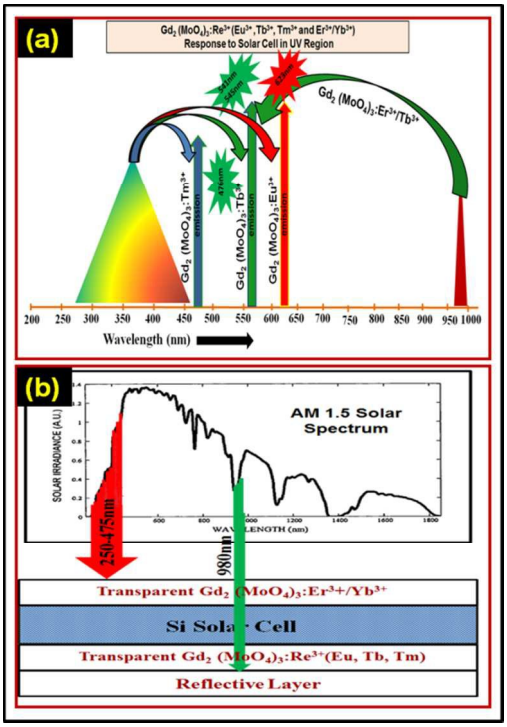

Fig. 6: (a) and (b) demonstrates the schematic diagram of proposed $Gd_2(MoO_4)_3:Re^{3+}(Re^{3+}$ =Eu^{3+}, Tb^{3+}, Tm^{3+} and Er^{3+}/Yb^{3+}) nanophosphor (downshifts and upconversion) as a broad spectral converter from UV to NIR in order to enhanced the efficiency of Si-solar cell.

The $Gd_2(MoO_4)_3$:Eu^{3+} downshift nanophosphor can absorb photon of high energy in range of 250-475 nm and give strong red emission. The Si-solar cell cannot be utilised photons falling in this range of energy because of thermal losses. The $Gd_2(MoO_4)_3$:Eu^{3+}downshift nanophosphor can easily absorb the photons falling in this region and emits in visible spectrum region which can easily absorb by Si-solar cell for electron-hole pair generation. The NIR region is also not absorbed by solar cell because in NIR region solar cell is transparent. The $Gd_2(MoO_4)_3$:Er^{3+}/Yb^{3+}upconversion nanophosphor absorb NIR region and emits in visible spectrum region which can easily absorbed by Si-solar cell. Therefore, the efficiency of Si-solar cell could be enhanced by coating a thin layer of downshift nanophosphor in front side and upconversion nanophosphor layer on back side of Si solar cell. The Figs. 6 (a &b) demonstrate the proposed spectral converter for $Gd_2(MoO_4)_3$:Re^{3+}(Re^{3+} =Eu^{3+}, Tb^{3+}, Tm^{3+} and Er^{3+}/Yb^{3+}) nanophosphor in order to enhanced the efficiency of Si-solar cell. Thus, the obtained spectroscopy results reveal that the $Gd_2(MoO_4)_3$:Re^{3+}(Re^{3+}=Eu^{3+},Tb^{3+},Tm^{3+} and Er^{3+}/Yb^{3+}) nanophosphor could be a good choice as spectral converter for upcoming next generation Si-solar cell application.

4. Conclusions

We have successfully synthesized $Gd_2(MoO_4)_3$:Re^{3+}(Re^{3+} = Eu^{3+}, Tb^{3+} and Tm^{3+}) (downshift) and $Gd_2(MoO_4)_3$:Er^{3+}/Yb^{3+} (upconversion) nanophosphors by customized solid state reaction method which can be easily scale-up in large quantity. The structural and microstructure studies exhibit that nanophosphor have orthorhombic crystal structure with average size in the range of ~24-28 nm. The $Gd_2(MoO_4)_3$ has advantage over other host matrix that the excitation band is broad due the charge transfer in O-Mo in UV spectrum region, which is sufficiently transferred energy to trivalent lanthanide ions. The $Gd_2(MoO_4)_3$:Eu^{3+}downshiftnanophosphor demonstrates hypersensitive red emission at 616 nm corresponding to excitation in the range of 250-475 nm. The $Gd_2(MoO_4)_3$:Er^{3+}/Yb^{3+}upconversionnanophosphor shows strong green emission at 545 nm upon an excitation of 980 nm. The co-doping of Yb^{3+}ions assistance for the broad absorption in NIR region due to the Yb^{3+}ion can absorbs broad NIR region as compared to the Er^{3+}ion. Furthermore, $Gd_2(MoO_4)_3$:Er^{3+}/Yb^{3+}upconversionnanophosphor demonstrates emission at 994 nm, which is merely reported. Moreover, the TRPL spectroscopy demonstrates a PL lifetime in τ_{av}~0.64 ms which is assured the potential applications of the proposed nanophosphor as a broad spectral converter. Thus, the obtained PL and TRPL spectroscopy results of synthesized nanophosphor legitimates its potential use as a broad spectral converter for next generation Si-solar cells.

Notes and references

[a]*CSIR - National Physical Laboratory, Dr K S Krishnan Road, New Delhi, 110012, India*

[b]*Academy of Scientific and Innovative Research (AcSIR), CSIR –National Physical Laboratory, New Delhi – 110012, India*

** Corresponding author. Tel.: +91-11-45609385, Fx: +91-11-45609310*

*E-mail address: **bipinbhu@yahoo.com***

† Electronic Supplementary Information (ESI) available: [details of any supplementary information available should be included here]. See DOI: 10.1039/b000000x/

‡ Footnotes should appear here. These might include comments relevant to but not central to the matter under discussion, limited experimental and spectral data, and crystallographic data.

Acknowledgment

The authors wish to thank Director, N.P.L., New Delhi, for his keen interest in the work. The authors are thankful to Prof. O. N. Srivastava (Banaras Hindu University, Varanasi) for his encouragement. Mr. Pawan Kumar gratefully acknowledged University Grant Commission (UGC), Govt. of India, for financial assistance under RGNF Research Fellowship, Award No. F1-17.1/2011-12/RGNF-SC-PUN-12604 /(SA-III/Website). The authors are grateful to the CSIR TAPSUN program providing PL mapping instrument facility.

References:

1. G. D. Scholes, G. R. Fleming, A. Olaya-Castro and R. Grondelle, *Nature Chem.*, 2011, **3**, 763-774.
2. N. S. Lewis and D. G. Nocera, *PNAS*, 2006,**103**, 15729-15735.
3. O. Morton, *Nature*, 2006, **443**, 19-22.
4. B. M. van der Ende, L.Aartsa and A. Meijerink, *Phys. Chem. Chem. Phys.*, 2009, **11**, 11081-11095.
5. X. Huang, S. Han, W. Huang and X. Liu, *Chem. Soc. Rev.*, 2013, **42**, 173-201.
6. A. J. Nozik and J. Miller, *Chem. Rev.*, 2010, **110**, 6443-6445.
7. H. A. Atwater and A.Polman, *Nature Mater.*, 2010, **9**, 205-213.
8. P. K. Nayak, G. G. Belmonte,A. Kahn, J.Bisquert and D.Cahen, *Energy Environ. Sci.*, 2012, 5, 6022–6039.
9. A. Goetzberger, C. Hebling and H. W. Schock,*Mater. Sci. Eng.*, 2003, **40**, 1-46.
10. B. van der Zwaan and A. Rabl, *Solar Energy*, 2003, **74**, 19-31.
11. B.S. Richards, *Solar Energy Mater. Solar Cells*, 2006, **90**, 2329-2337.
12. O. M. ten Kate, M. de Jong, H. T. Hintzen and E. van der Kolk, *J. App. Phys.*, 2013, **114**, 084502.
13. C. Strumpela, M. McCann, G. Beaucarne, V. Arkhipov, A. Slaoui, V. Svrcek,C. del Canizo and I. Tobias, *Solar Energy Mater. Solar Cells*, 2007, **91**, 238-249.
14. T. Trupke, M. A. Green and P. Würfel, *J. App. Phys.*, 2002,**92**, 4117.
15. H. Q. Wang, M. Batentschuk, A. Osvet, L. Pinna and C. J. Brabec,*Adv. Mater.*, 2011, **23**, 2675-2680.
16. S. F. H. Correia, V. de Z. Bermudez, S. J. L. Ribeiro, P. S. Andre, R. A. S. Ferreira and L. D. Carlos, *J. Mater. Chem. A*, 2014, **2**,5580-5596.
17. W. Guo, K. Zheng,W. Xie,L. Sun,L. Shen,C. Liu, Y. He and Z. Zhang,*Solar Energy Mater. Solar Cells*, 2014, **124**, 126-132.

18. S. K. W. MacDougall, A. Ivaturi, J. Marques-Hueso, K. W. Krämerand B. S. Richards, *Solar Energy Mater. Solar Cells*, 2014, **128**, 18-26.
19. M. G. Debije and P. P. C. Verbunt, *Adv. Energy Mater.*, 2012, **2**, 12-35.
20. J. de Wild, A. Meijerink, J. K. Rath, W. G. J. H. M. van Sark and R. E. I. Schropp, *Energy Environ. Sci.*, 2011, **4**, 4835-4848.
21. E. Klampaftis, D. Ross, K. R.McIntosh and B. S. Richards, *Solar Energy Mater. Solar Cells*, 2009, **93**, 1182-1194.
22. W. G.J.H.M. van Sark, *Renew. Energy*, 2013, **49**, 207-210.
23. P. F.Scudo, L. Abbondanza,R. Fusco and L. Caccianotti, *Solar Energy Mater. Solar Cells*, 2010, **94**, 1241-1246.
24. X. Liu, L. Li, H. M. Noh, B. K. Moon, B. C. Choib and J. H. Jeong, *Dalton Trans.*, 2014, **43**,8814-8825.
25. B. K. Gupta, D. Haranath, S. Saini, V. N. Singh and V.Shanker, *Nanotechnol.*, 2010, **21**, 055607.
26. S. Abtmeyer, R. Pązik,R. J. Wiglusz,M. Małecka, G. A. Seisenbaeva, V. G. Kessler, Inorg. Chem. 2014, **53**, 943–951
27. A. Dwivedi, A. K.Singh and S. B. Rai, *Dalton Trans.*, 2014,**43**,15906.
28. T. V. Gavrilovic, D. J. Jovanovic, V. Lojpur and M. D. Dramicanin, *Sci. Rep.*, 2014, **4**, 4209.
29. B. K. Gupta, N. N. Tharangattu, S. A. Vithayathil, Y. Lee, S. Koshy, A. L. M. Reddy, A. Saha, V. Shanker, V. N. Singh, B. A. Kaipparettu, A. A.Martí, and P. M.Ajayan, *Small*, 2012, **8**, 3028-3034.
30. M. Haase and H. Schafer, *Angew. Chem. Int. Ed.*, 2011, **50**, 5808-5829.
31. A. Shalav, B. S. Richards, T. Trupke, K. W. Krämer and H. U. Güdel, *App. Phys. Lett.*, 2005, **86**, 013505.
32. D. Chen, L. Lei, A. Yang, Z. Wang and Y. Wang, *Chem. Commun.*, 2012, **48**, 5898-5900.
33. A.C. Pana, C. del Canizo, E. , N. M. Santos, J. P. Leitao and A. Luque, *Solar Energy Mater. Solar Cells*, 2010, **94**, 1923-1926.
34. K. Mishra, S. K. Singh, A. K. Singh, M. Rai, B. K. Gupta andS. B. Rai, *Inorg. Chem.*, 2014, **53**, 9561-9569.
35. F. Lahoz, C. P. Rodrıguez, S.E.Hernandez, I.R.Martın, V.Lavın and U.R.R. Mendoza, *Solar Energy Mater. Solar Cells*, 2011, **95**, 1671-1677.
36. Y. Y. Cheng, B. Fuckel, R. W. MacQueen, T. Khoury, R. G. C. R. Clady,T. F. Schulze, N. J. E. Daukes, M. J. Crossley, B. Stannowski, K. Lipsand T. W. Schmidt, *Energy Environ. Sci.*, 2012, **5**, 6953-6959

Cite this: DOI: 10.1039/c0xx00000x

www.rsc.org/xxxxxx

RESEARCH ARTICLE

Graphical Table of Contents (TOC)

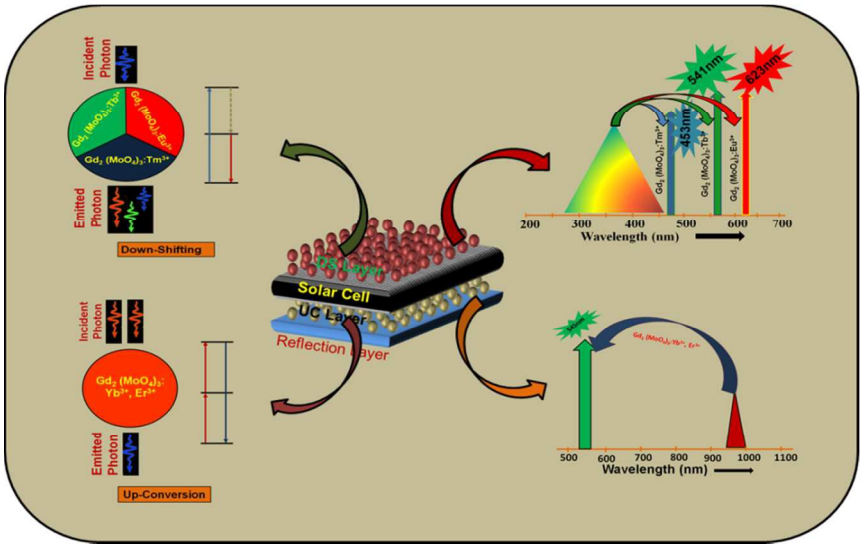

Demonstration of novel rare-earth doped gadolinium molybdate nanophosphor assisted broad spectral converter from UV to NIR for Si-solar cell applications.